JOURNAL OF MOLECULAR SPECTROSCOPY 80, 86–108 (1980)

Analysis of Perturbations in the $A^2\Pi$–$X^2\Sigma^+$ "Red" System of CN

ANTHONY J. KOTLAR, ROBERT W. FIELD, AND JEFFREY I. STEINFELD

Department of Chemistry and Spectroscopy Laboratory, Massachusetts Institute of Technology, Cambridge, Massachusetts 02139

AND

JOHN A. COXON

Department of Chemistry, Dalhousie University, Halifax, Nova Scotia B3H 4J3, Canada

Deperturbed vibration–rotation constants of the $A^2\Pi$ ($v' = 0$ to 12) and $X^2\Sigma^+$ ($v'' = 0$ to 8) states of CN are obtained. Spectroscopic data from several sources are combined using a weighted, nonlinear least-squares fitting routine. The diagonalized effective Hamiltonian matrix contains as many as two $^2\Pi$ and four $^2\Sigma^+$ mutually interacting vibronic levels. Perturbations of $A^2\Pi$ by both $X^2\Sigma^+$ and $B^2\Sigma^+$ are treated simultaneously. The deperturbed constants and interaction matrix elements obtained provide a significantly more accurate representation of all perturbed and unperturbed observed lines than the previously reported values. The electronic factors of the spin–orbit and rotation–electronic perturbation matrix elements for the $A \sim X$ and $A \sim B$ interactions are determined and several previously unreported perturbations are detected and analyzed. Merged constants and Dunham coefficients are calculated; a detailed statistical treatment of the parameters and error estimates has also been carried out.

I. INTRODUCTION

The "Red" band system of CN, arising from transitions between the $A^2\Pi$ and the $X^2\Sigma^+$ states of this radical, has been the subject of numerous investigations (for a summary of the literature through 1973, see (*1*)). Several reports (*2*,*3*) already exist which catalog the data and survey the literature for this system. The Berkeley atlas (*3*), in particular, consists of some 10 000 measured frequencies divided among 39 vibrational bands, and represents the single most comprehensive tabulation of CN $A^2\Pi$–$X^2\Sigma^+$ transitions. Since its publication in 1963, two separate analyses (*4*,*5*) have been performed on these data. Neither of these studies analyzes all the transitions in the atlas and, in particular, the spectroscopic perturbations known to occur (*6*–*8*) in the A–X band system are treated in an unsatisfactory fashion. A number of developments have taken place since the most recent treatment of this system, which makes a reanalysis advisable. First, nonlinear least-squares fitting techniques have been developed (*9*–*12*) which make such an analysis feasible. Furthermore, some very high-quality Fourier transform spectroscopic data have been recorded (*13*), which provide greatly improved accuracy for many transitions, and extend the range of J values up to $J \sim 100$. By combining the earlier tabulation with these more recent data, and using the powerful fitting tech-

0022-2852/80/030086-23$02.00/0

niques now available, we can present here the most complete analysis of the best data presently available on the $A^2\Pi-X^2\Sigma^+$ system of CN, including a detailed perturbation analysis which includes both $A \sim X$ and $A \sim B$ interactions.

There are several reasons for such an analysis to be of interest at this time. One is the need for collisional quenching rates for the CN A state. Gelbart and Freed (*14*) have shown that the rate for collision-induced population redistribution involving states of mixed Π and Σ^+ character contains two contributions, one for electronic quenching ($\Pi \rightarrow \Sigma^+$), and a $\Pi \rightarrow \Pi$ transfer process resembling a rotational relaxation within the Π state. The contributions of these channels are proportional to $(1 - \rho^2)$ and ρ^2, respectively, where ρ^2 is the mixing fraction in the perturbed level. In previous studies (*15–17*) of collision-induced quenching in I_2 ($0_u^+ \sim 0_g^+$) and N_2 ($^3\Pi_g \sim {}^3\Delta_u$, $^3\Sigma_u^+$), the mixing fractions are zero in the absence of a collision, as a result of the g/u symmetry. Since one does not know the extent of the mixing of these states caused by breaking of the g/u symmetry during the collision, the value of ρ^2 can only be roughly estimated. In the case of CN($A^2\Pi$), however, the perturbations exist in the absence of collisions, since there is no inversion symmetry, and it is possible to calculate the mixing fractions and perturbation parameters from the spectroscopic data alone. Thus, there is no ambiguity about the magnitude of the coupling between perturbing states arising from the intramolecular interactions of the molecule.

A knowledge of quenching and energy transfer rates is required for understanding laser action involving the CN $A-X$ system. A parametric evaluation of electronic transition laser candidates by Sutton and Suchard (*18*) indicated that the CN $A-X$ system fulfilled many of the requirements for producing a chemically pumped, electronic transition laser. West and Berry (*19*) have, in fact, observed $A \rightarrow X$ lasing from CN following photodissociation of various cyanide parents. An $A \rightarrow X$ laser pumped by a pulsed electric discharge has also been reported (*20*), with efficiencies as high as 10%. Betts and Miller (*21*) have attempted to produce a chemically pumped $A \rightarrow X$ laser from reaction between F_2, D_2, and $(CN)_2$ or CNCl, but were unsuccessful in doing so. Collisional deactivation of the A-state CN produced in that reaction may have been partly responsible for their lack of success. Quenching rates are also needed for calibrating fluorescence probes of CN in atmospheric-pressure flames (*22, 23*). Recently, quenching rates have been reported for CN $A^2\Pi$ produced by photodissociation of HCN in collision with He, Ne, Ar, N_2, and H_2 (*24*). The quenching cross sections range from 0.004 to 0.14 Å^2. The authors of Ref. (*24*) suggest that collisions of CN($A^2\Pi$) with quenching gases may induce radiationless transitions to near-degenerate high-vibrational levels of the $X^2\Sigma^+$ state, as in the perturbation scheme discussed here.

A further application for the present analysis is in astrophysical measurements (*4, 5*). CN is an important constituent of solar and stellar atmospheres, and accurate spectroscopic constants are required to predict the positions of high-J lines and transitions involving isotopic (^{13}C, ^{15}N) species.

II. HAMILTONIAN

The effective Hamiltonian used in the present analysis of CN has been widely discussed (*9, 25–28*), and we present here only the definitions of those terms used

in our calculations. The Hamiltonian is

$$\mathcal{H} = \mathcal{H}_0 + \mathcal{H}^{\text{Rot}} + \mathcal{H}^{\text{fs}} + \mathcal{H}^{\text{hfs}} \tag{1}$$

$\mathcal{H}_0$ includes those terms of the Born–Oppenheimer approximation which are independent of rotation, and involves only the electronic and vibrational quantum numbers, n and v. We determine the vibronic term energy T_v separately for each band analyzed. The band-by-band results are later merged to yield a set of Dunham coefficients from which potential curves for the A and X states may be calculated. $\mathcal{H}^{\text{hfs}}$ includes the effect of the nuclear moments interacting with the electronic or magnetic fields of the molecule to produce the hyperfine structure. Since this structure is not observed in the optical transitions analyzed here, we need not consider it further.

The present analysis concentrates on $\mathcal{H}^{\text{Rot}}$, describing the rotation of the nuclei, and $\mathcal{H}^{\text{fs}}$, containing the magnetic terms giving rise to the fine structure interaction. $\mathcal{H}^{\text{Rot}}$ has the form

$$\mathcal{H}^{\text{Rot}} = B(R)\mathbf{R}^2 \tag{2a}$$

$$= B(R)(\mathbf{J} - \mathbf{L} - \mathbf{S})^2, \tag{2b}$$

where

$$B(R) = h/8\pi^2\mu R^2. \tag{3}$$

$B(R)$ is the radial part of the rotational energy operator, μ is the reduced mass of $^{12}C^{14}N$, and R is the internuclear distance.

The fine-structure Hamiltonian is composed in general of three parts

$$\mathcal{H}^{\text{fs}} = \mathcal{H}^{\text{SO}} + \mathcal{H}^{\text{SS}} + \mathcal{H}^{\text{SR}}, \tag{4}$$

where $\mathcal{H}^{\text{SO}}$ is the spin–orbit, $\mathcal{H}^{\text{SS}}$ the spin–spin, and $\mathcal{H}^{\text{SR}}$ the spin–rotation interaction. Since the spin–spin interaction is rigorously zero for all doublet states, it can be dispensed with in this analysis. The spin–orbit Hamiltonian has the simplified form, for $\Delta S = 0$ matrix elements only (*29*, *30*),

$$\mathcal{H}^{\text{SO}} = A\mathbf{L}\cdot\mathbf{S} \tag{5a}$$

$$= A[L_zS_z + \tfrac{1}{2}L_+S_- + \tfrac{1}{2}L_-S_+], \tag{5b}$$

where A is the spin–orbit coupling constant. The spin–rotation interaction is given by

$$\mathcal{H}^{\text{SR}} = \gamma(\mathbf{R}\cdot\mathbf{S}) \tag{6a}$$

$$= \gamma(\mathbf{J} - \mathbf{L} - \mathbf{S})\cdot\mathbf{S}, \tag{6b}$$

where γ is the spin–rotation constant. These expressions are all phenomenological forms for the terms of $\mathcal{H}^{\text{fs}}$ but have matrix elements identical with the correct forms.

We choose a basis set of Hund's case (a) wavefunctions. These wavefunctions are simultaneously eigenfunctions of J^2, S^2, J_z, S_z, and L_z, and have eigenvalues $J(J+1)$, $S(S+1)$, Ω, Σ, and Λ; the eigenvalue of L^2, however, is not specified. The total wavefunction is a product function $|nv\rangle\,|\Lambda\Sigma S\Omega J\rangle$. We carry out a further transformation to a basis set symmetrized with respect to reflection in the plane containing the internuclear axis (σ_v). The parity convention for half-integral spin

is (*31*)

$$e \text{ levels: } \sigma_v\psi = +(-1)^{J-1/2}\psi, \tag{7a}$$

$$f \text{ levels: } \sigma_v\psi = -(-1)^{J-1/2}\psi. \tag{7b}$$

The resulting symmetrized wavefunctions [Eqs. (8a)–(8c)] are just those which are required in order to evaluate the effective Hamiltonian for $^2\Sigma^+$ and $^2\Pi$ states, the only states needed in this analysis of CN.

$$^2\Sigma^+_{1/2}\begin{pmatrix} e \\ f \end{pmatrix} = \frac{1}{2^{1/2}}\{|^2\Sigma_{1/2}\rangle \pm |^2\Sigma_{-1/2}\rangle\}, \tag{8a}$$

$$^2\Pi_{3/2}\begin{pmatrix} e \\ f \end{pmatrix} = \frac{1}{2^{1/2}}\{|^2\Pi_{3/2}\rangle \pm |^2\Pi_{-3/2}\rangle\}, \tag{8b}$$

$$^2\Pi^+_{1/2}\begin{pmatrix} e \\ f \end{pmatrix} = \frac{1}{2^{1/2}}\{|^2\Pi_{1/2}\rangle \pm |^2\Pi_{-1/2}\rangle\}. \tag{8c}$$

Of primary interest in this analysis are the operators $J_\pm L_\mp$ (arising from $\mathscr{H}^{\text{Rot}}$) and $L_\pm S_\mp$ (from $\mathscr{H}^{\text{Rot}}$ and $\mathscr{H}^{\text{SO}}$), since they couple states of different electronic character, and cause the mixing of their zero-order wavefunctions. The result of this mixing is known as a "perturbation," and is described by two parameters (*32*)

$$\alpha \equiv \tfrac{1}{2}\langle \Pi, v'|AL_+|\Sigma, v\rangle, \tag{9}$$

$$\beta \equiv \langle \Pi, v'|B(R)L_+|\Sigma, v\rangle, \tag{10}$$

with A and $B(R)$ defined by Eqs. (5) and (3), respectively. The form of Eqs. (9) and (10) indicates that the perturbation couples different electronic states through both a spin–orbit (A) and rotation–electronic (B) interaction.

Up to this stage in its development, the effective Hamiltonian matrix consists of blocks which are diagonal in J and which represent $^2\Sigma^+$ and $^2\Pi$ states (one block for each and every vibrational level of each $^2\Sigma^+$ and $^2\Pi$ state) with the perturbation matrix elements α and β coupling all the appropriate blocks (i.e., $^2\Sigma^+ \sim {}^2\Pi$). In general, nonzero matrix elements will also be found for $\Pi(v) \sim \Pi(v')$ and $\Sigma(v) \sim \Sigma(v')$ interactions. These matrix elements are off-diagonal in v, but couple states of the same electronic character. Ignoring all these perturbations, for the time being, we see that each $^2\Sigma^+$ state is a 2×2 block [Eq. (8a)] and each $^2\Pi$ state is a 4×4 block [Eqs. (8b), (8c)] of the original $n \times n$ matrix, with each block representing a pure Born–Oppenheimer state. The choice of the e/f parity basis functions, however, allows each block to be factored into two submatrices, with the appropriate submatrix being labeled as either an e or an f parity block. If the perturbation and other off-diagonal matrix elements are once again considered, then the Born–Oppenheimer blocks are coupled and the original $(n \times n)$ matrix must be evaluated. This matrix, however, will also factor into two $((n/2) \times (n/2))$, e/f matrices, since the perturbations obey the selection rules $e \leftrightarrow e, f \leftrightarrow f$, and couple only states of the same parity.

Second-Order Effects

Rather than attempting to obtain the eigenvalues of such a large matrix, we instead apply the methods of perturbation theory. We use the Van Vleck transfor-

TABLE I

Definitions of Second-Order Parameters Used in this Analysis

Parameters	Definitions	Types of Interactions
D_v	$-\sum_{v'} \frac{\lvert\langle v'\rvert B\rvert v\rangle\rvert^2}{E_v - E_{v'}}$	$\Sigma(v') \sim \Sigma(v)$ $\Pi(v') \sim \Pi(v)$
p_v	$2 \sum_{v'} \frac{\langle v\rvert A\, L_+\rvert v'\rangle\langle v\rvert BL_+\rvert v'\rangle}{E_v - E_{v'}}$	$\Sigma(v') \sim \Pi(v)$ $\Sigma(v) \sim \Pi(v')$
q_v	$2 \sum_{v'} \frac{\lvert\langle v\rvert BL_+\rvert v'\rangle^2}{E_v - E_{v'}}$	$\Sigma(v') \sim \Pi(v)$ $\Sigma(v) \sim \Pi(v')$
γ_{Dv}	$\sum_{v'} \frac{\langle v\rvert\gamma\rvert v'\rangle\langle v\rvert B\rvert v'\rangle}{E_v - E_{v'}}$	$\Sigma(v') \sim \Sigma(v)$ $\Pi(v') \sim \Pi(v)$
A_{Dv}	$2 \sum_{v'} \frac{\langle v\rvert A\rvert v'\rangle\langle v\rvert B\rvert v'\rangle}{E_v - E_{v'}}$	$\Pi(v') \sim \Pi(v)$

mation (*33*) to "fold in" the combined effects of distant perturbers as a correction to the matrix elements of the Born–Oppenheimer states. Nine new parameters evolve from this treatment when second-order corrections to the Hamiltonian are considered (*9*). Four of these are either very small or are highly correlated with other parameters, and are not evaluated in practice. The remaining five, considered in this analysis, are D, the quartic centrifugal distortion coefficient; p and q, the Λ-doubling constants; γ_D, the centrifugal distortion correction to γ; and A_D, the centrifugal distortion correction to A. Definitions of these parameters will be found in Table I. Noting the origin of these parameters (i.e., types of interaction), we see that the Λ-doubling constants arise from $\Sigma \sim \Pi$ interactions while the other parameters arise from both $\Sigma \sim \Sigma$ and $\Pi \sim \Pi$ interactions.

Higher-Order Effects

The Van Vleck transformation can be applied to produce higher-order terms; in practice, only those are retained which are centrifugal distortion corrections to those parameters already forming part of the Hamiltonian. The terms used in our analysis are H, the sextic centrifugal distortion coefficient; p_D and q_D, centrifugal distortion corrections to the Λ-doubling constants; γ_H, third-order centrifugal distortion correction to γ; and A_H, third-order centrifugal distortion correction to A. In general, these third-order constants are defined in accordance with the appropriate term of the Van Vleck transformation expansion. For the case of the third-order centrifugal distortion coefficient H, for example, this gives

$$H \equiv \sum_{v' \neq v} \cdot \sum_{v'' \neq v} \frac{\langle v|B|v'\rangle\langle v'|B|v''\rangle\langle v''|B|v\rangle}{(E_v - E_{v'})(E_v - E_{v''})} - \langle v|B|v\rangle \sum_{v' \neq v} \frac{|\langle v|B|v'\rangle|^2}{(E_v - E_{v'})^2}, \quad (11)$$

which, along with D, is exactly the same form given by the result of the Rayleigh–Schrödinger nondegenerate perturbation theory (*34*). This theory has been used to calculate values of the centrifugal constants, D, H, and L (fourth order), from a rotationless RKR potential (*35*).

From the deluge of terms coming from fourth order we mention only q_H, the third-order centrifugal distortion correction to the Λ-doubling constant, which was included, but not well determined, in fitting the Fourier transform data. One is here (if not sooner) in that grey area of the effective Hamiltonian, where the physical significance of many of the terms becomes obscure and, in reality, a parameter is retained for the sole purpose of introducing a particular J-dependence into the Hamiltonian matrix elements.

Several alternative definitions of these higher-order terms have appeared in the literature. We use the expansion in $J(J + 1)$ discussed by Coxon (*36*) for some of the higher-order terms in this analysis. The matrix elements of the terms in the Hamiltonian are given explicitly in Table II, where only those terms have been included which have actually been evaluated, or held at constant values, in the fit. The variable J has been used explicitly in addition to x ($=J + \frac{1}{2}$), to further indicate where the $J(J + 1)$ expansion has been used. General expressions for many of these matrix elements have recently been given by Brown *et al.* (*37*).

Near-Degenerate Perturbations (Crossings)

When the perturbation matrix elements are large or the energy difference between levels is small or, especially, when the levels actually cross, then the results of nondegenerate perturbation theory may no longer adequately account for the interaction between the specific states. When this happens, the near degenerate perturbing level is removed from the Van Vleck theory summations (see Table I), and is treated explicitly in the Hamiltonian. As many of these perturbing states as are necessary can be included in the Hamiltonian. The matrix elements of the Hamiltonian comprising the original Born–Oppenheimer state include second- and higher-order effects, added via the Van Vleck transformation. We now explicitly include, as additional states, all the near-degenerate or strongly perturbing levels. These levels are themselves Born–Oppenheimer states whose matrix elements have been adjusted by addition of the Van Vleck theory perturbation parameters.

Figure 1 gives an overall view of the relationship of the various energy levels of the X, A, and B states. Since only those levels having the same value of J (and parity) perturb each other, and since the effects of the perturbations are larger when the energy difference between levels is small, we can use Fig. 1 as a kind of "road map" for indicating why specific levels were chosen as interacting in our analysis. We emphasize that Fig. 1 is not intended to convey more than a general description of the crossings since, in fact, each level of the X state is really two levels (an e and f parity level) and each level of the A state is really four levels (an e and f parity level for each of the two spin–orbit components) for a given value of J. A more detailed view of the actual crossings, and a listing of where they occur, is given below in Section VB.

TABLE II

Hamiltonian Matrix Elements for $^2\Sigma^+$ and $^2\Pi$ states†

E	(0,0)=1 (1,1)=1 (2,2)=1	γ_D	(0,0)=$-\frac{1}{2}(1\mp x)J(J+1)$
		γ_H	(0,0)=$-\frac{1}{2}(1+x)J^2(J+1)^2$
A	(1,1)=$\frac{1}{2}$ (2,2)=$-\frac{1}{2}$	α	(0,2)=1
B	(0,0)=$x(x\mp1)$ (1,1)=x^2-2 (1,2)=$-(x^2-1)^{\frac{1}{2}}$ (2,2)=x^2	β	(0,1)=$-(x^2-1)^{\frac{1}{2}}$ (0,2)=$1\mp x$
		p_D	(1,2)=$-\frac{1}{2}(x^2-1)^{\frac{1}{2}}J(J+1)$ (2,2)=$\frac{1}{2}(1\mp x)J(J+1)$
D	(0,0)=$x^2(x\mp1)^2$ (1,1)=$(1-x^2)-(x^2-2)^2$ (1,2)=$2(x^2-1)^{3/2}$ (2,2)=$(1-x^4)-x^2$	q_D	(1,1)=$\frac{1}{2}(x^2-1)J(J+1)$ (1,2)=$-\frac{1}{2}(1\mp x)(x^2-1)^{\frac{1}{2}}J(J+1)$ (2,2)=$\frac{1}{2}(1\mp x)^2J(J+1)$
p	(1,2)= $-\frac{1}{4}(x^2-1)^{\frac{1}{2}}$ (2,2)=$\frac{1}{2}(1\mp x)$	q_H	(1,1)=$\frac{1}{2}(x^2-1)J^2(J+1)^2$ (1,2)=$-\frac{1}{2}(1\mp x)(x^2-1)^{\frac{1}{2}}J^2(J+1)^2$ (2,2)=$\frac{1}{2}(1\mp x)J^2(J+1)^2$
q	(1,1)=$\frac{1}{2}(x^2-1)$ (1,2)=$-\frac{1}{2}(1\mp x)(x^2-1)^{\frac{1}{2}}$ (2,2)=$\frac{1}{2}(1\mp x)^2$	H	(0,0)=$x^3(x\mp1)^3$ (1,1)=$(x^2-2)^3+3(x^2-1)^2-x^3+1$ (1,2)=$-(x^2-1)^{\frac{1}{2}}[3(x^2-1)^2+x^2]$ (2,2)=$x^6+3(x^2-1)^2+x^2-1$
A_D	(1,1)=x^2-2 (2,2)=$-x^2$		
γ	(0,0)=$-\frac{1}{2}(1\mp x)$		

†Letting $0 \rightarrow {}^2\Sigma^+$, $1 \rightarrow {}^2\Pi_{3/2}$ and $2 \rightarrow {}^2\Pi_{1/2}$, the matrix elements are constructed by summing over the appropriate interaction; $x \equiv J + \frac{1}{2}$.

III. FITTING PROCEDURE

A weighted, nonlinear, least-squares fitting routine is used to carry out this analysis (*9–12*, *38*, *39*). This program accepts either transition frequencies (F_i) or term energies as input data, along with initial guesses of the spectroscopic constants and estimated experimental standard deviations for each datum (σ_i). Only transition frequencies were used as input data in this analysis. The initial values of the parameters of each band are used to evaluate the Hamiltonian matrix, which is then diagonalized. The resulting eigenvalues form a table of term energies from which calculated transitions are obtained. These calculated transitions are then compared to the experimentally observed frequencies. Corrections to the parameters are computed, and a new table of term energies is constructed using the

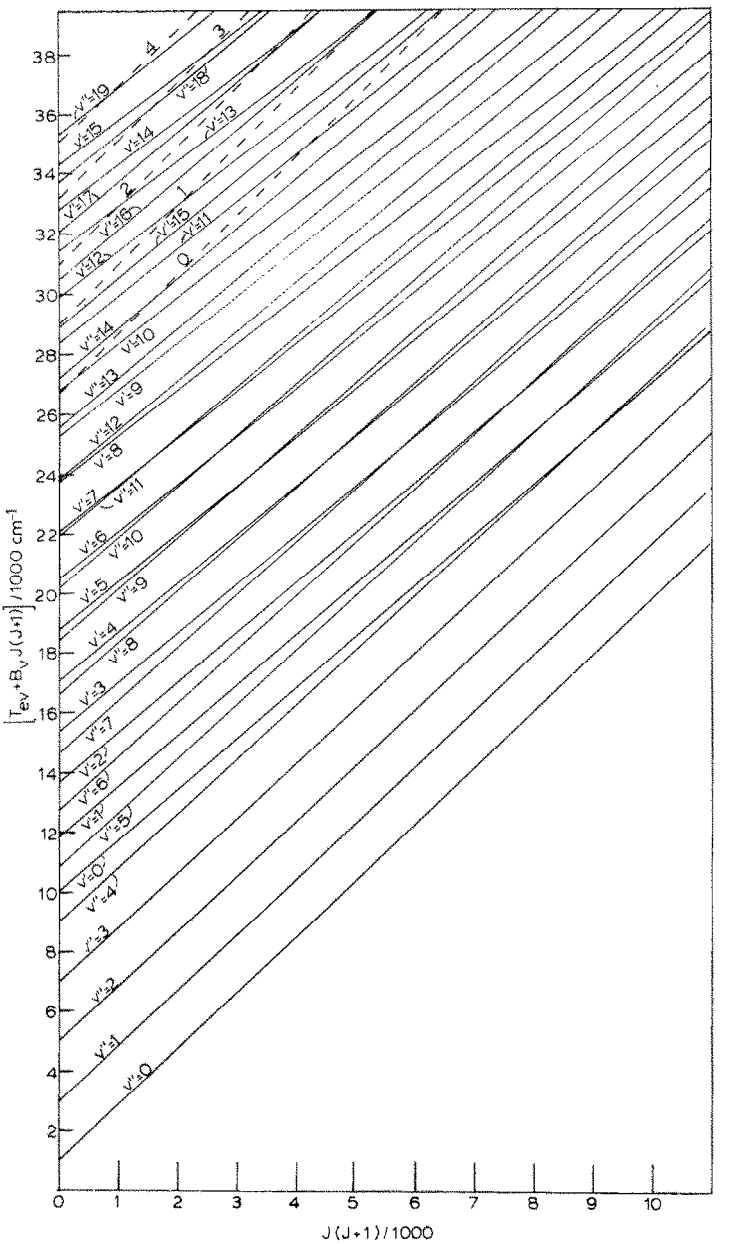

FIG. 1. Overall view of the energy levels for $X^2\Sigma^+(v'')$, $A^2\Pi(v')$, and $B^2\Sigma^+$. The B state is indicated by the broken lines, with the single number denoting the vibrational level.

adjusted parameter values. This procedure is repeated until convergence is achieved.

One of the advantages of using this kind of fitting procedure, over the customary "combination differences" approach, is that *all* the data of a band are used to fit

all the parameters simultaneously. This can be seen more clearly by briefly examining the way in which the corrections to the parameters are calculated. The matrix equation

$$\mathbf{A}\boldsymbol{\delta} = \mathbf{g} \tag{12}$$

is constructed, where **A**, the curvature or normal equation matrix, is dimensioned $m \times m$, where m is the number of parameters being fit, $\boldsymbol{\delta}$ is a vector of the corrections which are to be subtracted from the parameters, and **g** is the gradient or error vector. **A** has elements

$$a_{jk} = \sum_{i=1}^{N} w_i \frac{\partial f_i}{\partial b_j} \frac{\partial f_i}{\partial b_k}, \qquad j = 1, \ldots m, \qquad k = 1, \ldots m, \tag{13}$$

where N is the number of input data, b is the parameter, and $f = f(J)$ is the value of the function being evaluated (the transitions or term energies) at the current value of the parameters. The weights, w_i, are computed as the reciprocal of the square of the estimated experimental uncertainties, $w_i = 1/\sigma_i^2$. Matrix **A** only samples the range of the data (J values), and contains no information about the accuracy of the computed function. Vector g has elements

$$g_j = \sum_{i=1}^{N} w_i (f_i - F_i) \frac{\partial f_i}{\partial b_j}, \qquad j = 1, \ldots m, \tag{14}$$

where F_i is the experimental value of the ith datum; **g** contains all the information about the goodness of the fit. We see that both **A** and **g** involve summations over all the data points and have members which correspond to each of the parameters being varied.

Matrix **A** and vector **g** are then scaled,

$$\mathbf{A}^* = (a_{ij}^*) = \left(\frac{a_{ij}}{a_{ii}^{1/2} a_{jj}^{1/2}} \right), \tag{15}$$

$$\mathbf{g}^* = (g_i^*) = \left(\frac{g_i}{a_{ii}^{1/2}} \right), \tag{16}$$

where the asterisk denotes the scaled quantities. Equation (12) (with **A** and **g** scaled, i.e., **A*** and **g***) is now solved for the corrections $\boldsymbol{\delta}^*$, which are descaled

$$\delta_i = \delta_i^* / a_{ii}^{1/2} \tag{17}$$

and subtracted from the parameter values.

If the scaled curvature matrix **A*** is inverted, the result is a matrix of correlation coefficients of the errors among the parameters. This matrix is usually referred to simply as the correlation matrix. Descaling the correlation matrix and multiplying by the variance $\hat{\sigma}^2$ [Eq. (19)] produces the variance/covariance matrix,

$$\mathbf{C} = \hat{\sigma}^2 (a_{ij}^*)^{-1} / (a_{ii}^{1/2} a_{jj}^{1/2}). \tag{18}$$

The square roots of the diagonal elements of this matrix are the standard deviations of the parameters. The scaled curvature matrix **A*** can also be diagonalized. This corresponds to a transformation to a set of new parameters which are functions

of the original parameters, and with the eigenvectors indicating the linearly independent parameter combinations. The data can, at best, only determine these linearly independent parameter combinations. Nevertheless, one can simply examine these eigenvalues after the manner of Lees (*40*), to discover if any parameters are being varied which, in fact, should be removed from the fit. Marquardt's algorithm (*41*) is used to facilitate calculation of the correction vector.

A convenient measure of the progress of a band toward convergence is the variance

$$\hat{\sigma}^2 = \frac{1}{N - m} \sum_{i=1}^{N} \frac{(F_i - f_i)^2}{\sigma_i^2}, \tag{19}$$

where F_i is the experimental transition frequency (ν_i), f_i is its calculated value with the current set of parameters, and the other quantities have already been defined in this section. For a typical CN band, where $N \simeq 300$ and $m \simeq 10$, if each transition is on the average being fit to within its estimated experimental uncertainty (i.e., $F_i - f_i \simeq \sigma_i$), then the variance $\hat{\sigma} \simeq 1$.

Following analysis of all the individual bands, a merging procedure (*12*, *42*) was used to determine a single best set of values of the spectroscopic constants for each level. Eleven bands from the FTS data (*13*) were merged with twenty-seven bands from the Berkeley atlas (*3*), using the "stepwise merge" procedure developed by Coxon (*42*). These bands span the region $0 \leq v'' \leq 7$ and $0 \leq v' \leq 12$. Several bands were excluded from the merge; the details are discussed further in Section V.

IV. DATA SOURCES

The data set to which we refer as the Berkeley bands is contained in the atlas compiled by Davis and Phillips at the University of California at Berkeley (*3*). The atlas comprises 39 bands of the $A^2\Pi$–$X^2\Sigma^+$ system ranging from $v'' = 0$ to 8 and $v' = 0$ to 12, 15. This compilation plus an additional 55 transitions of the (2,1) band which, although not contained in Ref. (*3*), were included on the tape containing the data sent to us by Prof. Phillips, were analyzed using the procedures outlined in the preceding section. In order to achieve convergence in most of the bands, it was necessary to reject certain transitions either because they involved nonexistent levels, $(F_i - f_i)$ was greater than $5\sigma_i$, or, in some rare instances, because large systematic errors were apparent. We chose a standard deviation for the transitions of $\pm 0.02\ \text{cm}^{-1}$, as recommended by Davis and Phillips for unblended lines; we assumed a standard deviation 10 times this value for transitions identified in the atlas as blends ($\pm 0.20\ \text{cm}^{-1}$). This gives a ratio of weights of 100:1 for unblended/blended lines. In all, 10 753 transitions were analyzed of which 48 were reassigned and 481 were totally removed from the fit.

The Fourier transform spectroscopy (FTS) data set consisted of 3686 measured lines comprising 14 vibrational bands with $v' = 0$–4, $v'' = 0$–4. The data, especially for transitions between the lower v levels, are of very high quality ($\sigma_i = \pm 0.0017\ \text{cm}^{-1}$). We have taken a somewhat different approach in treating this data set in comparison to the Berkeley data. Both a global and band-by-band fit had already produced a good set of spectroscopic constants for these bands (*13*). As a result

of this analysis, all questionable lines had already been removed from the data set. It was not necessary for us, therefore, to reject any of the lines during our fit. We were interested, however, in including the effect of the $A \sim X$ perturbations, since these had *not* been considered in the previous analysis. As a result, we started with a good set of spectroscopic constants, added the perturbations, and allowed all the bands to reconverge.

Some high-precision data from microwave spectroscopic studies are also available. Meakin and Harris (*43*) have determined values of the perturbation coefficients α and β [Eqs. (9) and (10)] for $A^2\Pi$ ($v' = 10$) and $B^2\Sigma^+$ ($v = 0$). Their values, $\alpha_{10,0} = -0.3961$ cm^{-1} and $\beta_{10,0} = 0.0268$ cm^{-1}, have been chosen as fixed parameters in the analysis of the (10,3), (10,4), and (10,5) bands. More recent ODMR measurements by Cook and Levy (*44*) give revised values of $\alpha_{10,0} = -0.0868$ cm^{-1} and $\beta_{10,0} = 0.0357$ cm^{-1}. Although these two sets of parameters reproduce the zero-field data, caution should be exercised in extrapolating the results of this analysis above $v' = 10$. The correspondence between the perturbation parameters α and β defined here and those of Refs. (*43*) and (*44*) is

$$\alpha \equiv \langle \Pi | \, | AL_x | \, | \Sigma \rangle \langle v_\Pi | v_\Sigma \rangle,$$

$$\beta \equiv \langle \Pi | \, | L_x | \, | \Sigma \rangle \langle v_\Pi | B | v_\Sigma \rangle.$$

In our fits to levels of $A^2\Pi$ for $v' \geq 10$, we used a value of β which was too small by a factor of 2. Due to the small size of the $B \sim A$ perturbations for the fitted ($v' = 10$ to 12) levels, we believe that this error had a negligible effect on the fitted constants.

Values of B and γ for $v'' = 0$ and 1 are also available from microwave absorption studies (*45*), and are compared with the results of this analysis in the following section.

V. RESULTS

A. *Spectroscopic Constants*

In the first stage of this analysis, sets of constants which reproduce each individual band were determined. The results for the (7,2) band may be regarded as typical, and are illustrated by the output shown in Table III. The perturber of $v' = 7$ is $v = 11$ of the X state, indicated in brackets. Thirteen parameters are varied in this fit, including B, D, and γ for the ($X^2\Sigma^+$, $v'' = 2$) level, and T_v, A, B, D, q, and p for the ($A^2\Pi$, $v' = 7$) level. The perturbation parameters α ($v_\Pi = 7$, $v_\Sigma = 11$) $= -6.20$ cm^{-1} and β ($v_\Pi = 7$, $v_\Sigma = 11$) $= +0.032$ cm^{-1} are also determined, as are T_v and B for the ($X^2\Sigma^+$, $v = 11$) perturbing level; D and γ for the latter state are not determined, but are held fixed. The variance is 1.065, which indicates that the 331 measured transitions are being fitted, on the average, to within their standard deviation.

Once fitted values of α and β are obtained for one pair of interacting states, their values for other sets of interacting levels can be calculated and held at these values in the fit if the data do not permit their being independently varied. This was done for all levels of the A state, although for $v' = 0$, 1, and 2 of the Berkeley data all the retained lines in the fit which included the effects of the perturbation could also be

TABLE III

Spectroscopic Constants Derived for the CN (7,2) Band
CN $A^2\Pi(1)$–$X^2\Sigma^+(1)(7,2)$/Davis/$\langle X^2\Sigma^+(2)\ v = 11\rangle$

NUMBER	NAME	FINAL VALUE	STANDARD DEVIATION	
	E1S	0.5089690000D+04		1/CM
1	B1S	0.1855818121D+01	0.7134E-04	1/CM
2	D1S	0.6340262808D-05	0.1913E-07	1/CM
3	GAM1S	0.6700299089D-02	0.2341E-03	1/CM
4	E1P	0.2212499369D+05	0.4118E-02	1/CM
5	B1P	0.1584983268D+01	0.7090E-04	1/CM
6	A1P	-0.5199823928D+02	0.8742E-02	1/CM
7	Q1P+	-0.4371084133D-03	0.3389E-05	1/CM
8	D1P	0.6175850888D-05	0.1875E-07	1/CM
9	P1P+	0.7552867962D-02	0.2642E-03	1/CM
10	B1P2S	0.3187200139D-01	0.3967E-03	1/CM
11	A1P2S	-0.6200821503D+01	0.2674E-01	1/CM
12	E2S	0.2204355505D+05	0.3757E-01	1/CM
13	B2S	0.1696520672D+01	0.2093E-03	1/CM
	D2S	0.6000000000D-05		1/CM
	GAM2S	0.5000000000D-02		1/CM

INPUT DATA: 331

VARIANCE OF THE FIT 0.1065339224867779D+01

RMS:	0.6400220340D-01	STD DEV:	0.6529732086D-01	1/CM
WRMS:	0.2894803214D-01	WSTD DEV:	0.2953381044D-01	1/CM

adequately accounted for by fixing the perturbation parameters at zero. For $v' = 8$, values of α and β could be determined directly for two of the bands, 8–3 and 8–5. For $v' = 10$ through 15, perturbations arise from $A \sim B$ as well as $A \sim X$ interactions. The perturbation matrix elements for $A^2\Pi$ ($v' \geq 10$) $\sim B^2\Sigma^+$ ($v \geq 0$) could not be determined from the Berkeley data alone. We have included this effect by using values of α and β obtained from microwave Zeeman spectroscopy (*43*, *44*). Based on these experimental values, we have calculated parameters for all the $B \sim A$ interactions, and have held those values fixed in the fit as well.

The FTS data set (*13*) is an important addition to CN spectroscopy and to our analysis of the perturbations. The precision and range of these data have permitted us to evaluate one of the perturbation parameters, α, for the (0,0) band. The result, α ($v_\Pi = 0$, $v_\Sigma = 4$) $= -0.67$, is within 0.8% of the value calculated from the data from the $v' = 7$ bands of the Berkeley compilation. This is an important check on the internal consistency of the perturbation parameters. Values of α were also determined for the (3,3) and (4,4) bands.

Several of the bands in the Berkeley atlas cannot be regarded as having been well fit, on the basis of their variances. The worst case is that of the (6,0) band, for which $\hat{\sigma}^2 = 4.8$, rather than 1.0–1.5 as for most of the other bands in this compilation. We observed, as did Poletto and Rigutti in their analysis (*4*), that the data for this band was of exceptionally poor quality; almost 50% of the originally listed transitions had to be discarded from our analysis. It would be preferable to use values of the constants for $v' = 6$ and $v'' = 0$ obtained from other bands to reconstruct the (6,0) spectrum, rather than those determined by fitting this band itself.

The individual constants for all of the 53 bands analyzed in this work are available as a supplement to this article[1]; Table III is a typical example.

A set of merged constants was produced by using 38 bands spanning the ranges $0 \leq v'' \leq 7$, $0 \leq v' \leq 12$. First, 11 of the FTS bands (13) were merged to produce 80 constants ($\hat{\sigma} = 2.55$). The (2–3) band was omitted from this step, since its inclusion raised the value of $\hat{\sigma}$ to 3.53. An attempt to merge these results with the 9 Berkeley bands spanning the same (v',v'') range (0 through 4) resulted in $\hat{\sigma} = 7.34$, indicating that the two data sets were not compatible. This is not surprising, since the FTS data had been analyzed with a somewhat different model including higher-order distortion constants (A_D, p_D, q_D, γ_D, H, etc.) than the Berkeley data. Furthermore, several branches which are resolved in the FTS data appear only as blended lines in the Berkeley bands. We therefore omitted from the merge the 9 Berkeley bands with *both* v' and $v'' \leq 4$, and proceeded to merge the remaining 27 bands (with the exception of the (6–4)), using the FTS results to "anchor" the constants for low v' and v''. The results of the 38-band merge are represented by 167 constants ($\hat{\sigma} = 3.73$).

We wished to reduce as many as possible of these terms, tabulated as individual values for each v' and v'', to coefficients in a Dunham expansion in $(v + \frac{1}{2})^k$. This was accomplished for the vibrational term values G_v and the rotational constants B_v and D_v for the $X^2\Sigma^+$ and $A^2\Pi$, and the spin–orbit constant A_v for the $^2\Pi$ state. These results are shown in Table IV, along with E_0 and B_0 for the $B^2\Sigma^+$ state, determined from the perturbation analysis. The expansion used is of the usual form

$$G_v = \sum_{k=0}^{k_{\max}} Y_{k0}(v + \tfrac{1}{2})^k, \tag{20a}$$

$$B_v = \sum_{k=0}^{k_{\max}} Y_{k1}(v + \tfrac{1}{2})^k, \tag{20b}$$

and so on, so that $Y_{20} = -\omega_e X_e$, $Y_{11} = -\alpha_e$, etc.; T_e' is tabulated as Y_{00}'.

Initially, the spin–rotation constants γ_v'' and the lambda-doubling constants p_v' and q_v' were not constrained to a Dunham expansion; these are given in Table V. The higher-order distortion coefficients (H, γ_D, A_D, etc.) are also given as functions of v' and v'' in Table VI. Some of these, such as γ_D, γ_H, and q_H, are not really determined by this fit. These tables include 103 independent constants reproducing the data with a variance of 4.62. It was found possible to fit γ, p, and q to expressions linear in $(v + \frac{1}{2})$, reducing the number of constants to 75 and increasing the variance to only 4.96. None of the other constants changed as a result of these additional constraints by an amount greater than the standard error listed in Tables IV and VI. The resulting expressions (all in cm^{-1}) are

$$\gamma_v = 7.243(50) \times 10^{-3} - 1.29(22) \times 10^{-4}(v + \tfrac{1}{2}), \tag{21a}$$

$$p_v = 8.462(57) \times 10^{-4} - (5.38 \pm 2.83) \times 10^{-5}(v + \tfrac{1}{2}), \tag{21b}$$

$$q_v = -3.862(14) \times 10^{-4} - 6.10(61) \times 10^{-6}(v + \tfrac{1}{2}). \tag{21c}$$

[1] Anyone interested in this supplement should first write to the authors directly. If for some reason they cannot be reached, a few copies of this material are on deposit in the Editorial Office.

TABLE IV

Merged Vibration–Rotation Constants for CN $X^2\Sigma^+$ and $A^2\Pi$ States (cm^{-1})[a]

	$X^2\Sigma^+ (0 \leq v'' \leq 7)$			$A^2\Pi$ $(0 \leq v' \leq 12)$			
	Y''_{K0}	Y''_{K1}	Y''_{K2}	Y'_{K0}	A'_K	Y'_{K1}	Y'_{K2}
K=0	0	1.899729(10)	$6.3860(29)\times10^{-6}$	9 245.017(4)[b]	-52.6846(21)	1.715882(10)	$6.1286(30)\times10^{-6}$
1	2 068.690(6)	$-1.73774(42)\times10^{-2}$	$(7.86\pm1.11)\times10^{-9}$	1 813.267(8)	$6.86(22)\times10^{-2}$	$-1.72208(49)\times10^{-2}$	$(6.89\pm1.14)\times10^{-9}$
2	-13.126(4)	$-2.29(18)\times10^{-5}$	$(1.6\pm3.2)\times10^{-9}$	-12.774(5)	$3.35(23)\times10^{-3}$	$-2.65(23)\times10^{-5}$	$(1.21\pm0.14)\times10^{-9}$
3	$(-4.3\pm1.1)\times10^{-3}$	$(-8.0\pm2.3)\times10^{-7}$		$(-2.95\pm1.04)\times10^{-3}$			
4	$(-1.84\pm0.99)\times10^{-4}$			$(1.63\pm0.99)\times10^{-4}$			
5				$(-1.36\pm0.33)\times10^{-5}$			

[a]The figure in parentheses is the standard error in the last digit(s): when the relative standard error is ± 15% or more, the notation ($x \pm \sigma$) is used instead.

[b]This is T'_e for the A state.

$B^2\Sigma^+$ state: $E(v = 0) = 26\ 834.99(6)\ cm^{-1}$

$B_0 = 1.922(51)\ cm^{-1}$

TABLE V

Spin–Rotation, Lambda-Doubling, and Perturbation Constants for CN $X^2\Sigma^+$ and $A^2\Pi$ States (all in cm^{-1})[a]

v	$\gamma_v'' \times 10^3$	$p_v' \times 10^3$	$-q_v' \times 10^4$	$\alpha(v_\Pi, v_\Sigma)$	$\beta(v_\Pi, v_\Sigma)$	(v_Π, v_Σ)
0	7.19(4)	8.42(5)	3.892(13)	-0.67(10)		0,4
1	7.07(6)	8.55(14)	3.994(30)			
2	6.95(10)	8.45(14)	4.070(44)			
3	6.79(10)	9.20(49)	4.065(100)	-0.97(68)		3,7
4	6.74(10)	7.51(55)	4.104(105)	-4.18(41)		4,8
5	5.70(46)	7.51(30)	4.032(47)			
6	3.82(90)	7.44(52)	4.069(93)			
7	5.55±1.79	7.56(38)	4.188(54)	-6.24(4)	0.0329(9)	7,11
8		8.32(52)	4.327(73)	-6.87(3)	0.0381(37)	8,12
9		8.82(56)	4.63(10)			
10		7.95(80)	4.96(14)			
11		10.1±1.1	5.13(19)			
12		8.9±1.7	6.17(32)			

[a]See footnote (a), Table IV.

The results of this analysis compare quite well with the microwave spectroscopy results (*45*), to wit:

Parameter	Microwave value (cm^{-1})	Value calculated from Table IV and V
B_0''	1.8910782(2)	1.89104_2
γ_0''	$7.25455(10) \times 10^{-3}$	$7.19_4 \times 10^{-3}$
B_1''	1.8736542(10)	1.87361_2
γ_1''	$7.1753(10) \times 10^{-3}$	$7.07_6 \times 10^{-3}$

The values derived for Y_{01}'', Y_{11}', and Y_{21}'' are equally consistent.

B. Perturbations

The perturbations considered in this analysis are those arising from the crossing or near degeneracy of energy levels in two different electronic manifolds. These have been taken into account in the Hamiltonian by explicitly including the interacting states coupled by the perturbation matrix elements α and β. In those cases where the data did not suffice to fit α or β for the $A \sim X$ interaction, these constants were held fixed at values calculated from the $v' = 7$ bands. To calculate these fixed values, we note that both α and β are composed of an electronic part which, if as-

TABLE VI

Higher-Order Distortion Constants for CN $X^2\Sigma^+$ and $A^2\Pi$ States (cm^{-1})[a]

	$X^2\Sigma^+$			$A^2\Pi$				
	$H''\times10^{12}$	$\gamma_D''\times10^{9}$	$\gamma_H''\times10^{13}$	$H'\times10^{12}$	$A_D'\times10^{5}$	$p_D'\times10^{7}$	$q_D'\times10^{8}$	$q_H'\times10^{14}$
v=0	4.84(24)	(-9.±10)	(-4.±39.)	2.53(24)	1.46(13)	-2.71(11)	1.07(5)	-8.±6.
1	4.48(24)	0.4±32.0		1.48(28)	1.23(34)	-3.52(68)	1.19(12)	
2	3.77(26)	9.8±42.0		1.28(25)	1.34(29)	-3.96(51)	1.18(26)	4.±39.
3	2.93(40)				0.28±0.70	(-10.5±3.4)	1.14(56)	
4	0.88±0.69							

[a]See footnote (a), Table IV.

sumed constant, can be factored out. We can then write these vibronic matrix elements as the product of a vibrational and an electronic matrix element.

$$\alpha = \langle v_\Sigma | v_\Pi' \rangle \left\langle \Sigma \left| \frac{A}{2} L_+ \right| \Pi \right\rangle = \langle v_\Sigma | v_\Pi' \rangle \mathscr{H}_{el}^{SO}, \tag{22}$$

$$\beta = \left\langle v_\Sigma \left| \frac{1}{\Pi^2 \mu R^2} \right| v_\Pi' \right\rangle \langle \Sigma | L_+ | \Pi \rangle = \langle v_\Sigma | B | v_\Pi' \rangle \mathscr{H}_{el}^{RE}, \tag{23}$$

where $\mathscr{H}_{el}^{SO}$ and $\mathscr{H}_{el}^{RE}$ denote the perturbations arising from the spin–orbit and rotation–electronic interactions, respectively. The vibrational integrals $\langle v | v' \rangle$ and $\langle v | 1/R^2 | v' \rangle$ are calculated numerically from RKR potential curves for the $X^2\Sigma^+$, $A^2\Pi$, and $B^2\Sigma^+$ states.

The nature of the four level crossings for the $A^2\Pi \sim X^2\Sigma^+$ interaction is shown in Fig. 2. This figure is an expanded view of the crossings which were represented in Fig. 1 as single levels. We see that the crossings occur at various values of J, with the $^2\Pi_{3/2}(f) \sim {}^2\Sigma^+(f)$ always being the lowest while the $^2\Pi_{1/2}(e) \sim {}^2\Sigma^+(e)$ crossing is always at the highest value of J. The order of the other two crossings varies, depending on the interacting vibrational levels. An important product of this analysis is the mixing fraction (ρ^2) of the interacting levels. In Table VII, we list the J values at which the crossings occur, along with the maximum mixing fractions and corresponding J values for each interaction. The mixing fractions indicate that the perturbation is actually strongest for the $v' = 6 \sim v'' = 10$ interaction, where the $^2\Pi_{3/2}(e)$, $J = 44$ level is almost 48% of Σ character. We illustrate in Figs. 3 through 5 some measures (shift, percentage Σ character) of the strength of the perturbation as a function of J. Data from the (7,2) and (8,3) bands are used as being representative of the two cases encountered, that is, the levels actually crossing or the levels interacting as if a "crossing" had occurred at $J < 0$.

Figure 3 indicates the frequency shifts ($\Delta\nu = \nu_{pert} - \nu_{unpert}$) caused by perturbations in the two parity components of one of the A-state spin orbit components, namely, $^2\Pi_{1/2}$, $v' = 7$. Since α and β have different signs the strength of the per-

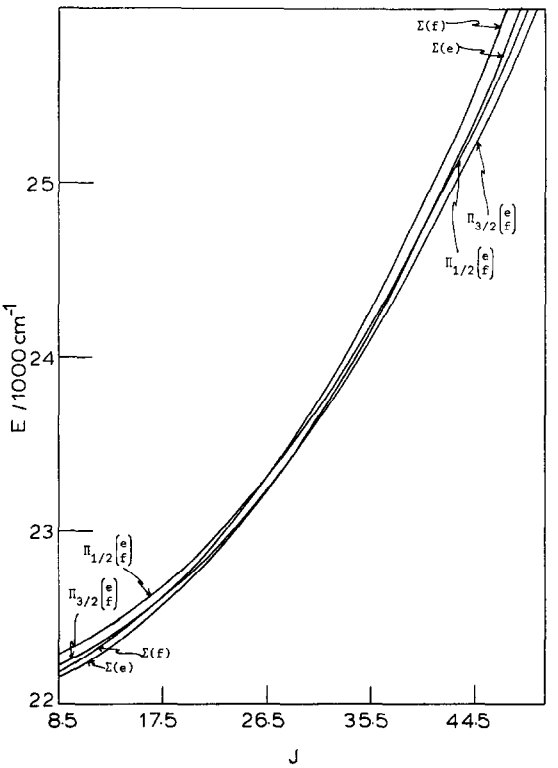

FIG. 2. Detail of level crossing, $A^2\Pi$ ($v' = 7$) ~ $X^2\Sigma^+$ ($v'' = 11$). The difference between the *e*/*f* parity components of the two spin–orbit components of the $^2\Pi$ state is less than 2 cm^{-1} over the range of J shown; data from the (7,2) band.

turbation can, in a given case, be small even though both α and β are large. Also, some of the $^2\Sigma \sim {}^2\Pi_{1/2}$ matrix elements are parity- and J-dependent; thus, it is not surprising that the *e* and *f* levels should be affected differently by the perturbation. For the levels in Fig. 3 the difference in level shift between the perturbations of *e* vs *f* levels is not large. The most strongly perturbed *e* level is shifted by about 4 cm^{-1} from its expected location in the absence of any perturbations.

Figures 4 and 5 show the dependence of the mixing of the interacting levels as a function of J. In Fig. 4, a comparison of the extent of the mixing of the two spin–orbit components (same parity) for $v' = 7$ is presented. In Fig. 5, the mixing of the different parity levels of the same spin–orbit component, $\Pi_{1/2}$, $v' = 8$ are shown. $\Pi_{1/2}$ is more strongly perturbed than $\Pi_{3/2}$ in this case, since the Σ state lies at higher energy; that is, the perturbation of $A^2\Pi$ is from above (for $v' = 8$), rather than from below (for $v' = 0$ to 7). The perturbation is such that it is not valid to consider the interaction merely as if the crossing had occurred at a "negative J" value. This can be seen in Fig. 5, where the mixing coefficient rises to a maximum at $J = 11\frac{1}{2}$ and only then decreases monotonically as J increases.

Using Eqs. (22) and (23), we can summarize the results of the perturbation analysis for the $A \sim X$ interaction in terms of the reduced matrix elements $\mathscr{H}_{el}^{SO}$

TABLE VII

Level Crossings and Maximum Σ Character for Components of $A^2\Pi$ State

v'',v ($X^2\Sigma^+$,$B^2\Sigma^+$) [f]	v' ($A^2\Pi$)	$\Pi_{3/2} \sim \Sigma$						$\Pi_{1/2} \sim \Sigma$					
		e parity levels			f parity levels			e parity levels			f parity levels		
		J_{cross} [a]	J_{max} [b]	Σ_{max} [c]	J_{cross}	J_{max}	Σ_{max}	J_{cross}	J_{max}	Σ_{max}	J_{cross}	J_{max}	Σ_{max}
4	0	98.5	99.5	1.9	84.5	84.5	0.4	d	d	d	98.5	d	d
5	1	91.5	91.5	3.0	77.5	77.5	1.7	d	d	d	90.5	91.5	0.03
6	2	89.5	90.5	16.2	72.5	73.5	3.8	d	d	d	88.5	89.5	1.9
7	3	76.5	76.5	19.2	62.5	62.5	10.4	92.5	92.5	5.1	75.5	76.5	0.05
8	4	67.5	67.5	35.5	53.5	53.5	13.8	83.5	84.5	12.2	66.5	67.5	4.3
9	5	57.5	57.5	26.9	46.5	44.5	22.5	74.5	74.5	23.0	57.5	57.5	35.8
10	6	44.5	44.5	47.9	30.5	31.5	34.8	62.5	62.5	41.3	44.5	44.5	39.6
11	7	24.5	25.5	42.8	12.5	13.5	42.6	44.5	44.5	34.4	26.5	26.5	31.7
12	8	e	19.5	0.1	e	14.5	0.03	e	10.5	5.4	e	0.5	2.9
13	9	e	28.5	0.03	e	21.5	0.01	e	7.5	0.2	e	0.5	0.2
14,$\underline{0}$	10	6.5	6.5	2.3	1.5	2.5	0.9	15.5	15.5	2.5	9.5	10.5	23.9
15,$\underline{\frac{0}{1}}$	11	52.5	52.5	8.9	47.5	48.5	0.1	55.5	56.5	0.2	51.5	51.5	0.1
16,$\underline{\frac{1}{2}}$	12	45.5	45.5	0.8	41.5	42.5	0.1	49.5	49.5	1.1	44.5	44.5	0.8
19 18,$\underline{3}$	15	60.5	60.5	36.0	50.5	51.5	15.5	69.5	70.5	9.3	54.5	60.5	0.8

[a] J value immediately before the crossing

[b] J value having maximum Σ character

[c] Σ character of Π state (%)

[d] $J > 100$ and/or $\%\Sigma < 0.0005$

[e] $J < 0$

[f] vibronic level for which crossing J-value is tabulated is underlined

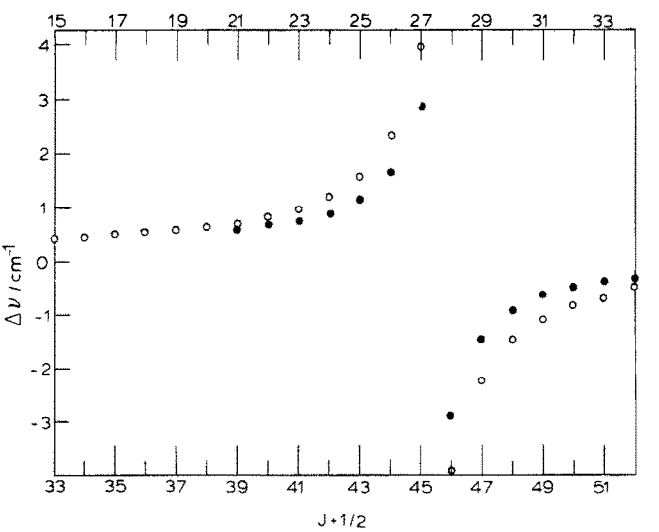

FIG. 3. $\Delta\nu = (\nu_{perturbed} - \nu_{unperturbed})$ vs $J + \frac{1}{2}$ for e (○) and f (●) parity levels of $A^2\Pi_{1/2}$ ($v' = 7$); data from the (7,2) band.

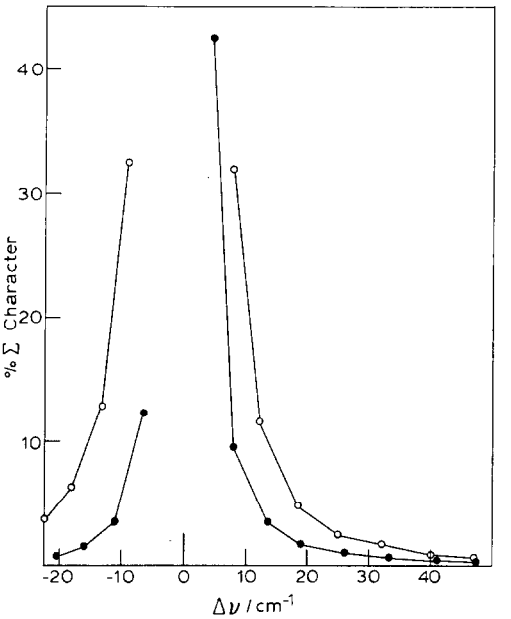

FIG. 4. Percentage Σ character vs $\Delta\nu = (\nu_\Sigma - \nu_\Pi)$ for f parity levels of $\Pi_{3/2}$ (●) and $\Pi_{1/2}$ (○) ($v' = 7$); data from the (7,2) band; the solid lines serve only to connect the points corresponding to different J values.

and $\mathscr{H}_{el}^{RE}$. The weighted average values of these quantities are

$$\mathscr{H}_{el}^{SO} = -(16.15 \pm 0.13)\ \text{cm}^{-1},$$
$$\mathscr{H}_{el}^{RE} = 0.0734 \pm 0.0024\ \text{cm}^{-1}.$$

The values of α from the $v' = 0, 3, 4, 7$, and 8 levels, and of β from the $v' = 7$ and 8 levels, have each been divided through by the appropriate vibrational integral, and the resulting reduced matrix elements averaged to obtain the above quantities. Consistent values of $\mathscr{H}_{el}^{SO}$ and $\mathscr{H}_{el}^{RE}$ were obtained from each measurement.

VI. DISCUSSION

The analysis presented here represents the most complete evaluation to date of all available CN spectroscopic data, including $A \sim X$ and $A \sim B$ perturbation interactions. The deperturbed constants, together with the perturbation terms which affect all A-state levels and all X-state levels with $v'' \geq 4$, reproduce the 14 000 measured transitions in this system with accuracy an order of magnitude greater than in either of the previous analyses (*4*, *5*). The variance accurately reflects the experimental error of the individual measurements. A nonrigorous estimate of the average absolute accuracy of calculated individual line frequencies can be obtained by multiplying the variance of the merged constants by the experimental uncertainty in measured line positions; this gives $\pm 0.008\ \text{cm}^{-1}$ for transitions with $v', v'' \leq 4, J \lesssim 100$. This predictive ability should be particularly

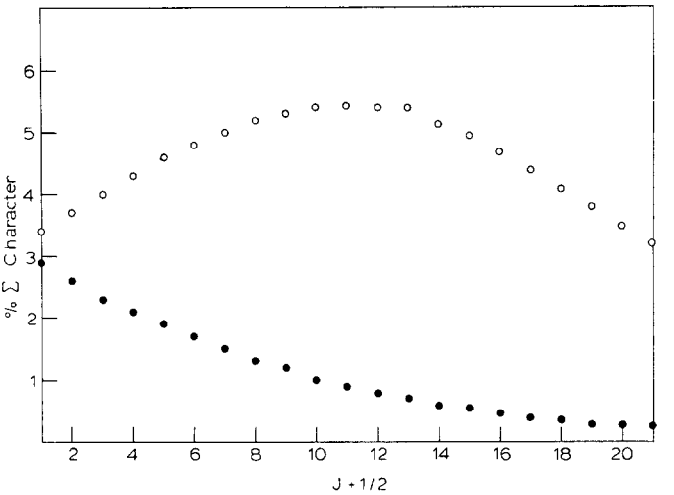

FIG. 5. Percentage Σ character vs $J + \frac{1}{2}$ for e (○) and f (●) parity levels of $A^2\Pi_{1/2}$ ($v' = 8$); data from the (8,3) band.

useful in studies of the solar spectrum, in which it is necessary to predict the positions of lines in the CN Red bands for J up to ~150 and ^{13}C and ^{15}N isotopic species. Since perturbations have a profound effect on these bands,[2] and there is no such thing as a "typical" or "routine" treatment, the following detailed instructions are provided for the optimum use of the constants presented here in calculating transition frequencies for both observed and hitherto unobserved CN $A^2\Pi-X^2\Sigma^+$ transitions.

It is necessary to set up an effective Hamiltonian matrix for both the upper and lower levels for any $A-X$ (v',v'') band. The vibronic levels explicitly included in each matrix are determined by the specific v_A or v_X level and the desired range of J-values. The Hamiltonian should include the desired v_A or v_X level and all possible $B^2\Sigma$, $A^2\Pi$, and $X^2\Sigma$ perturbing levels. The relevant perturbers may be determined from a crossing diagram similar to that in Fig. 1. All vibrational levels that cross the main level between $J = \frac{1}{2}$ and the maximum J-value must be included. In addition, it is advisable to include the next higher and lower vibrational levels of each perturbing electronic state. The necessary perturbation matrix elements are computed by multiplying the electronic factors

	$A \sim X$	$A \sim B(44)$
$\alpha/\langle v_\Pi \mid v_\Sigma \rangle$	$-16.15\ cm^{-1}$	-8.9
$\beta/B_{v_\Pi v_\Sigma}$	$+0.0734$	$+1.36$

by vibrational factors computed from RKR potential curves derived using the merged constants in Table IV. The effective Hamiltonian should then be set up using the matrix element definitions in Table II, constants for the $X^2\Sigma$ and $A^2\Pi$ levels from Tables IV–VI (or from the band-by-band constants in the Supplement),

[2] In fact, most of the Berkeley bands break off at high J, just at the onset of a new perturbation.

and constants for the $B^2\Sigma$ levels from Ref. (*50*). Levels for which constants are not listed in Table V may be adequately represented by the γ_v, p_v, and q_v expansions in Eqs. (21a)–(21c). Although all constants obtained here were derived from observed levels of $^{12}C^{14}N$, we believe that the deperturbed and merged nature of these constants makes them suitable for prediction of spectra of other isotopes after applying the usual isotopic shift formulas. Of course, vibrational integrals used in the computation of perturbation parameters must be recalculated for the appropriate isotope.

It should be noted that the constants for $v_A \geq 10$ are calculated with the $A \sim B$ perturbation parameters of Meakin and Harris (*43*), which are not in good agreement with more recent values of Cook and Levy (*44*). Thus caution should be exercised in computing line frequencies where the $A \sim B$ perturbations become more significant, which is for $v_A \geq 12$. Hopefully, work in progress (*60*) on the CN Violet ($B^2\Sigma^+$–$X^2\Sigma^+$) system will resolve this remaining source of uncertainty.

A comparison of the perturbation matrix elements $\mathcal{H}_{el}^{SO}$ and $\mathcal{H}_{el}^{RE}$, found here for CN, with those for isoelectronic systems would provide useful information with regard to the electronic structure of these molecules. Unfortunately, an analysis of these systems, comparable in extent to the present work on CN, has not been carried out. A perturbation at $J' = 13\frac{1}{2}$ in the 4–0 band of the α system of BO ($A^2\Pi$–$X^2\Sigma^+$) was noted by Jenkins and McKellar (*51*) but no interaction constant was obtained, and more recent work (*52*), on the 0–2 band did not reveal any perturbations. Bulthuis and co-workers (*53*, *54*) found perturbations in the 8–0 band of the CO^+ A–X system ($J = 14\frac{1}{2}$) and in many J-levels of the 13–1 and 13–2 bands of this system. They identified the perturbing level as $v = 18$ of the $X^2\Sigma^+$ state, and found its location relative to $v' = 13$, but did not derive the coupling coefficients. More recent work (*55*) on the 2–0 band did not reveal any additional perturbations.

As a result of the inversion symmetry in N_2^+, no perturbations exist between the $A^2\Pi_u$ and $X^2\Sigma_g^+$ states. Analyses of the $B^2\Sigma_u^+ - X^2\Sigma_g^+$ first negative system have revealed numerous perturbations between vibrational levels of the B and A states (*56*–*59*), and parameters comparable to those found in the present study have been obtained in the most recent of these analyses (*59*). Work in progress (*60*) on the CN Violet bands should result in improved values for the corresponding perturbation parameters for CN, which affect high v' levels of the A state. Further work on these isoelectronic species, directed toward locating both $A \sim X$ and $A \sim B$ perturbations, should provide data of interest for comparison with molecular-structure calculations.

ACKNOWLEDGMENTS

This research was supported by the U. S. Air Force Office of Scientific Research, under Grant AFOSR-75-2758. We would like to thank Mr. Richard Gottscho of M.I.T. for helpful discussions, Dr. Roger Bacis of the University of Lyons for providing data and analyses in advance of publication, Professor J. G. Phillips of the University of California for providing a magnetic tape of the Berkeley CN atlas, and Dr. Robert Kurucz for providing computer time at the Smithsonian Astrophysical Observatory.

RECEIVED: February 8, 1979

REFERENCES

1. S. N. SUCHARD, Ed., "Spectroscopic Data," Vol. I, pp. 284–307, IFI/Plenum, New York, 1975.
2. B. BROCKLEHRUST, G. R. HÉBERT, S. H. INNANEN, R. M. SEEL, AND R. W. NICHOLLS, "Identification Atlas of Molecular Spectra. 8. The CN $A^2\Pi$–$X^2\Sigma^+$ Red System," York University, Toronto, 1971.
3. S. P. DAVIS AND J. G. PHILLIPS, "The Red System ($A^2\Pi$–$X^2\Sigma$) of the CN Molecule," University of California Press, Berkeley, 1963.
4. G. POLETTO AND M. RIGUTTI, *Nuovo Cimento* **39,** 519–530 (1965).
5. T. FAY, I. MARENIN, AND W. VAN CITTERS, *J. Quant. Spect. Radiat. Transfer* **11,** 1203–1214 (1971).
6. F. A. JENKINS, Y. K. ROOTS, AND R. S. MULLIKEN, *Phys. Rev.* **39,** 16–41 (1932).
7. A. T. WAGNER, *Phys. Rev.* **64,** 18–31 (1943).
8. N. H. KIESS AND H. P. BROIDA, *J. Mol. Spectrosc.* **7,** 194–208 (1961).
9. R. N. ZARE, A. L. SCHMELTEKOPF, W. J. HARROP, AND D. L. ALBRITTON, *J. Mol. Spectrosc.* **46,** 37–66 (1973).
10. D. L. ALBRITTON, A. L. SCHMELTEKOPF, AND R. N. ZARE, *in* "Molecular Spectroscopy, Modern Research" (K. Narahari Rao and C. W. Mathews, Eds.), Vol. II, pp. 1–67, Academic Press, New York, 1976.
11. D. L. ALBRITTON, A. L. SCHMELTEKOPF, W. J. HARROP, AND R. N. ZARE, *J. Mol. Spectrosc.* **67,** 157–184 (1977).
12. D. L. ALBRITTON, A. L. SCHMELTEKOPF, AND R. N. ZARE, *J. Mol. Spectrosc.* **67,** 132–156 (1977).
13. D. CERNY, R. BACIS, G. GUELACHVILI, AND F. ROUX, *J. Mol. Spectrosc.* **73,** 154–167 (1978); R. BACIS, D. CERNY, J. D'INCAN, G. GUELACHVILI, AND F. ROUX, *Astrophys. J.* **214,** 946–950 (1977).
14. W. M. GELBART AND K. F. FREED, *Chem. Phys. Lett.* **18,** 470–475 (1973).
15. B. GARETZ, M. RUBINSON, AND J. I. STEINFELD, *Chem. Phys. Lett.* **28,** 120–124 (1974).
16. B. A. GARETZ, L. L. POULSEN, AND J. I. STEINFELD, *Chem. Phys.* **9,** 385–391 (1975).
17. B. A. GARETZ, J. I. STEINFELD, AND L. L. POULSEN, *Chem. Phys. Lett.* **38,** 365–369 (1976).
18. D. G. SUTTON AND S. N. SUCHARD, *Appl. Opt.* **14,** 1898–1910 (1975).
19. G. A. WEST AND M. J. BERRY, *J. Chem. Phys.* **61,** 4700–4716 (1974).
20. C. R. QUICK, JR. AND C. WITTIG, *in* "Electronic Transition Lasers, I" (J. I. Steinfeld, Ed.), pp. 225–227, M.I.T. Press, Cambridge, Mass., 1976.
21. J. A. BETTS AND D. J. MILLER, *in* "Electronic Transition Lasers, II" (L. E. Wilson, S. N. Suchard, and J. I. Steinfeld, Eds.), pp. 198–205, M.I.T. Press, Cambridge, Mass., 1977.
22. E. M. BALEWICZ, P. J. PADLEY, AND R. E. SMITH, "Proceedings, 14th International Symposium on Combustion," p. 329, The Combustion Institute, Pittsburgh, 1972.
23. D. PUECHBERTY AND M. J. COTTEREAU, *Combust. Flame* **29,** 99–102 (1977).
24. E. N. TERESCHCHENKO, S. N. GOLOVKOVA, AND N. YA. DODONOVA, *Opt. Spektrosk.* **42,** 561–563 (1977); English transl., *Opt. Spectrosc.* **42,** 315–316 (1977).
25. T. A. MILLER, D. H. LEVY, AND A. CARRINGTON, *Adv. Chem. Phys.* **18,** 149 (1970).
26. R. MCWEENY AND B. T. SUTCLIFFE, "Methods of Molecular Quantum Mechanics," Appendix 4, pp. 287–298, Academic Press, New York, 1969.
27. T. ITOH, *Rev. Mod. Phys.* **37,** 159–165 (1965).
28. J. T. HOUGEN, "The Calculation of Rotational Energy Levels and Rotational Line Intensities in Diatomic Molecules," *Nat. Bur. Stand. U. S. Monogr.* **115** (1970).
29. I. KOVACS, "Rotational Structure in the Spectra of Diatomic Molecules," American Elsevier, New York, 1969.
30. R. J. M. BENNETT, *Monthly Not. Roy. Astron. Soc.* **147,** 35–46 (1970).
31. J. M. BROWN, J. T. HOUGEN, K.-P. HUBER, J. W. C. JOHNS, I. KOPP, H. LEFEBVRE-BRION, A. J. MERER, D. A. RAMSAY, J. ROSTAS, AND R. N. ZARE, *J. Mol. Spectrosc.* **55,** 500–503 (1975).
32. H. LEFEBVRE-BRION, *in* "Atoms, Molecules and Lasers," pp. 411–448, Intern. At. Energy Agency, Vienna, 1974.
33. J. H. VAN VLECK, *Phys. Rev.* **33,** (1929); O. M. JORDAHL, *Phys. Rev.* **45,** 87–97 (1934).
34. A. DALGARNO, *in* "Quantum Theory. I. Elements" (D. R. Bates, Ed.), Chap. V., Academic Press, New York, 1961.

35. D. L. ALBRITTON, W. J. JONES, A. L. SCHMELTEKOPF, AND R. N. ZARE, *J. Mol. Spectrosc.* **46,** 25–36 (1973).
36. J. A. COXON, *J. Mol. Spectrosc.* **58,** 1–28 (1975).
37. J. M. BROWN, M. KAISE, C. M. L. KERR, AND D. J. MILTON, *Mol. Phys.* **36,** 553–582 (1978).
38. A. J. KOTLAR, Ph.D. thesis, Massachusetts Institute of Technology, Cambridge, May, 1978.
39. Earlier forms of this program have been used in: R. C. STERN, R. H. GAMMON, M. E. LESK, R. S. FREUND, AND W. A. KLEMPERER, *J. Chem. Phys.* **52,** 3467–3482 (1970); R. H. GAMMON, R. C. STERN, AND W. KLEMPERER, *J. Chem. Phys.* **54,** 2151–2163 (1971); R. W. FIELD AND T. H. BERGEMAN, *J. Chem. Phys.* **54,** 2936–2948 (1971). For a general description of the method see W. E. WENTWORTH, *J. Chem. Ed.* **42,** 96–103 (1965).
40. R. M. LEES, *J. Mol. Spectrosc.* **33,** 124–136 (1970).
41. D. W. MARQUARDT, *J. Soc. Indust. Appl. Math.* **11,** 431 (1963).
42. J. A. COXON, *J. Mol. Spectrosc.* **72,** 252–263 (1978).
43. P. MEAKIN AND D. O. HARRIS, *J. Mol. Spectrosc.* **44,** 219–229 (1972).
44. T. J. COOK AND D. H. LEVY, *J. Chem. Phys.* **58,** 3547–3557 (1973).
45. T. A. DIXON AND R. C. WOODS, *J. Chem. Phys.* **67,** 3956–3964 (1977).
46. R. W. FIELD, S. G. TILFORD, R. A. HOWARD, AND J. D. SIMMONS, *J. Mol. Spectrosc.* **44,** 347–382 (1972).
47. R. W. FIELD, B. G. WICKE, J. D. SIMMONS, AND S. G. TILFORD, *J. Mol. Spectrosc.* **44,** 383–399 (1972).
48. R. W. FIELD, *J. Chem. Phys.* **60,** 2400–2413 (1974).
49. B. G. WICKE, R. W. FIELD, AND W. KLEMPERER, *J. Chem. Phys.* **56,** 5758–5770, (1972).
50. R. ENGLEMAN, JR., *J. Mol. Spectrosc.* **49,** 106–116 (1974).
51. F. A. JENKINS AND A. MCKELLAR, *Phys. Rev.* **42,** 464–486 (1932).
52. T. M. DUNN AND L. (K.) HANSON, *Can. J. Phys.* **47,** 1657–1659 (1969).
53. D. COSTER, H. H. BRONS, AND H. BULTHUIS, *Z. Physik* **79,** 787–822 (1932).
54. H. BULTHUIS, *Proc. Roy. Soc. Amsterdam* **38,** 604 (1935).
55. H. GAGNAIRE AND J. P. GOURE, *Can. J. Phys.* **54,** 2111–2117 (1976).
56. S. S. LAZDINIS AND R. F. CARPENTER, *J. Chem. Phys.* **59,** 5203–5204 (1973).
57. J. DUFAYARD, J. M. NEGRE, AND O. NEDELEC, *J. Chem. Phys.* **61,** 3614–3618 (1974).
58. A. M. BOUCHOUX AND J. P. GOURE, *Can. J. Phys.* **55,** 1492–1498 (1977).
59. R. A. GOTTSCHO, R. W. FIELD, K. A. DICK, AND W. BENESCH, *J. Mol. Spectrosc.* **74,** 435–455 (1979).
60. J. BRAULT AND R. ENGLEMAN, JR., to be published.